PCCP

Accepted Manuscript

ROYAL SOCIETY OF CHEMISTRY

www.rsc.org/pccp

Journal Name

ARTICLE TYPE

Cite this: DOI: 10.1039/xxxxxxxxxx

Excitons in poly(*para* phenylene vinylene): A quantum-chemical perspective based on high-level *ab initio* calculations†

Stefanie A. Mewes,[a] Jan-Michael Mewes,[a] Andreas Dreuw,[a] and Felix Plasser[a,b]

Received Date
Accepted Date

DOI: 10.1039/xxxxxxxxxx

www.rsc.org/journalname

Excitonic effects play a fundamental role in the photophysics of organic semiconductors such as poly(*para* phenylene vinylene) (PPV). The emergence of these effects is examined for PPV oligomers based on high level *ab initio* excited-state calculations. The computed many-body wavefunctions are subjected to our recently developed exciton analysis protocols to provide a qualitative and quantitative characterization of excitonic effects. The discussion is started by providing high-level benchmark calculations using the algebraic-diagrammatic construction for the polarization propagator in third order of perturbation theory (ADC(3)). These calculations support the general adequacy of the computationally more efficient ADC(2) method in the case of singly excited states but also reveal the existence of low-energy doubly excited states. In a next step, a series of oligomers with chains of two to eight phenyl rings is studied at the ADC(2) level showing that confinement effects are dominant for small oligomers, while delocalized exciton bands emerge for larger systems. In the case of the largest oligomer, the first twenty singlet and triplet excited states are computed and a detailed analysis in terms of the Wannier and Frenkel models is presented. The presence of different Wannier bands becomes apparent, showing a general trend that exciton sizes are lowered with increasing quasi-momentum within the bands.

1 Introduction

Poly(*para* phenylene vinylene) (PPV)[1–5] is an organic π-conjugated system with special electronic properties representing a prominent molecule in the rapidly advancing scientific field of organic electronics.[5–12] Its simple structure consisting of the two monomers phenylene and vinylene renders this molecule an ideal prototype to explore the relation between molecular structure and electronic properties. The theoretical investigation of this polymer is, however, challenging due to its large size and the involvement of complex electron correlation effects. Despite the large number of studies, there is not even qualitative consensus about the nature of the excitons. Estimates of the binding energy lie in the range from almost free charge carriers at 0.1 eV to strongly bound states at 1.0 eV.[13–17]

A wide range of computational studies of PPV have been performed in recent years covering such diverse methods as solid-state physics models,[15,18,19] semi-empirical methods,[7,20–23], density matrix renormalization group theory solving a Pariser-Parr-Pople model,[24,25] time-dependent density functional theory,[26–28] many-body Green's function theory,[29,30] correlated *ab initio* methods[31–33] and non-adiabatic dynamics.[34,35] These studies have elucidated the properties of this polymer from different, sometimes contradictory viewpoints. The reconciliation of these different viewpoints is arguably one of the most pressing issues in this field and could move our understanding of these systems forward considerably. The major dividing line may be drawn between the solid-state physics inspired methods and the quantum chemical methods. The former are formulated in terms of a correlated quasi-particle *electron-hole* wavefunction and possess the advantage of a direct connection to the picture of charge carriers, which are invoked for the understanding of electronic devices. The latter take full account of the molecular details, but are based on molecular orbitals and hence lack the direct connection to charge carriers.

In the following, a selection of quantum-chemical studies, that are best suited for a comparison with this work, are briefly summarized. As a consequence of the large system size, the first computational studies were performed using approximate, semi-

[a] *Interdisciplinary Center for Scientific Computing, Ruprecht-Karls University, Im Neuenheimer Feld 368, D-69120 Heidelberg, GERMANY.*
[b] *Institute for Theoretical Chemistry, University of Vienna, Währingerstr. 17, A-1090 Wien, AUSTRIA; E-mail: felix.plasser@univie.ac.at*

† Electronic Supplementary Information (ESI) available: Evaluation of approximate exciton size measure; *Electron-hole* correlation plots of the first four electronically excited states of $(PV)_nP$ oligomers with $n = 1,2,3$ calculated at the ADC(2)/SV(P) and ADC(3)/SV(P) levels of theory; Analysis of triplet excited states of $(PV)_nP$ ($n = 1,\ldots,7$): *electron-hole* correlation plots, excitation energies, excited-state descriptors. See DOI: 10.1039/b000000x/

empirical methods[7,20–23,36] such as the collective-electronic oscillator (CEO) and the Zerner's intermediate neglect of differential overlap (ZINDO) methods. These led to a coarse picture of excitonic wavefunctions and assignment of different bands in the excitation spectrum of PPV. Further studies reported the application of linear-response time-dependent density functional theory (TDDFT) to oligomers of PPV.[26–28] This method has the ability to describe excited states of fairly large systems with twenty repeat units and more. However, this comes at the cost of a strong dependency of the results on the functional choice and it has been shown that excitons can be fine-tuned from completely unbound electron-hole pairs to tightly bound quasi-particles depending on the functional.[27,37] Accurate multi-reference *ab initio* methods such as complete active space self-consistent field (CASSCF) and complete active space perturbation theory to second order (CASPT2) have only been applied to the smallest PPV oligomer, stilbene, for which the computational demand is feasible.[38,39] Although these high-level *ab initio* methods yield accurate results for small systems, their predictive power for the extended polymer is rather limited. Due to its lower computational cost, symmetry-adapted cluster-configuration interaction (SAC-CI) can afford the computation of small oligomers with up to four units.[33] In this respect, the compromise between accuracy and computational demand provided by the algebraic-diagrammatic construction for the polarization propagator of second order (ADC(2)) constitutes a great improvement.[31] In contrast to CAS-PT2 and SAC-CI, this *ab initio* method allows for a description of oligomers with up to eight phenyl rings, which closely resemble the polymer with respect to its electronic properties.[36] The calculated vertical excitation energies are in good agreement with experimental data and it has been shown that defects in the oligomer chain lead to exciton localization. In addition the one-particle transition density matrix has been visualized to interpret the excited states in terms of an *electron-hole* picture.

In this work we combine high-level *ab initio* calculations with elaborate exciton analysis tools to take advantage of, both, the molecular and quasi-particle viewpoints of excitation processes. This is realized by subjecting the computed excited-state wavefunctions to our recently developed exciton analysis[40–43] following previous ideas in literature.[21,22,44,45] A key quantity in this analysis is the interpretation of the one-particle transition density matrix as an effective exciton wavefunction. The major objectives of this study are (i) to provide a high-level *ab initio* benchmark for vertical excitation energies and exciton properties on third-order level of perturbation theory (ii) to emulate the emergence of exciton properties for sufficiently large π-systems, and (iii) to systematically characterize exciton bands, both qualitatively and quantitatively.

2 Analysis of correlated exciton wavefunctions

Excited-state computations of large molecular systems do not only require highly efficient methodology, but also the analysis of the resulting wavefunctions can be challenging. Usually, the response vectors of the excited states with respect to the ground-state molecular orbitals are analyzed and if many contributions are involved, the analysis can become quite tedious. Moreover, it is often overlooked that some properties of interest may not be directly deduced from the shapes of the orbitals at all but the decisive information lies in the phase of their superpositions. This situation for example becomes evident in the case of dimers where only a sign change differentiates between charge resonance and excitonic states,[41,43,46] and the situation becomes even more intricate for multimers as studied here. A solution is to move from the orbital representation of the excited state to the representation of a correlated *electron-hole* wavefunction $\chi_{exc}(r_h, r_e)$ as illustrated in Figure 1. Such a wavefunction is naturally given in Green's function theory and we have recently highlighted that in a quantum-chemical context the one-particle transition density matrix (1TDM) γ^{0I} between the ground and excited-state wavefunctions can be interpreted analogously.[40,41] In this picture, the exciton wavefunction is constructed as

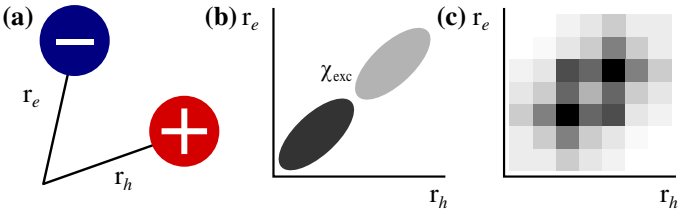

Fig. 1 Representation of the exciton wavefunction: (a) the *hole* and *electron* quasi-particles positioned at r_h and r_e, (b) the correlated exciton wavefunction χ_{exc} plotted against these coordinates, and (c) analysis of χ_{exc} in terms of an *electron-hole* correlation plot.

$$\chi_{exc}(r_h, r_e) := \gamma^{0I}(r_h, r_e) = N \int \dots \int \Phi^0(r_h, r_2, \dots, r_N)\Phi^I(r_e, r_2, \dots, r_N) dr_2 \dots dr_N, \quad (1)$$

where Φ^0 and Φ^I are the ground and excited-state many-body wavefunctions. In matrix representation, the 1TDM can be expressed as

$$\gamma^{0I}(r_h, r_e) = \sum_{\mu\nu} D^{0I}_{\mu\nu} \chi_\mu(r_h)\chi_\nu(r_e), \quad (2)$$

where χ_μ and χ_ν are atomic orbitals of the basis $\{\chi_\eta\}$ and the 1TDM element $D^{0I}_{\mu\nu}$ is defined as

$$D^{0I}_{\mu\nu} = \langle \Phi^0 | \hat{a}^\dagger_\mu \hat{a}_\nu | \Phi^I \rangle \quad (3)$$

with $\hat{a}^\dagger_\mu$ and $\hat{a}_\nu$ being the usual one-particle creation and annihilation operators. Using this construction, the exciton wavefunction is a readily available quantity that can be subjected to a variety of analyses. One particularly instructive analysis is to partially integrate over the square of γ^{0I}, while restricting the *hole* coordinate to one fragment A and the *electron* to a fragment B:

$$\Omega_{AB} = \int_A \int_B \gamma^{0I}(r_h, r_e)^2 \, dr_e dr_h. \quad (4)$$

The resulting so-called charge-transfer numbers[47] afford the probability to find the *hole* on fragment A, while the *electron* is located at B. Subjecting Eq. (4) to a Mulliken population analysis

leads to the working equation[40]

$$\Omega_{AB} = \frac{1}{2}\sum_{\mu\in A}\sum_{\nu\in B}\left[(\mathbf{D}^{0I}\mathbf{S})_{\mu\nu}(\mathbf{S}\mathbf{D}^{0I})_{\mu\nu} + D^{0I}_{\mu\nu}(\mathbf{S}\mathbf{D}^{0I}\mathbf{S})_{\mu\nu}\right], \quad (5)$$

where $\mathbf{S}$ is the overlap matrix between the basis functions.

We have recently extended our methodology to the computation of expectation values of arbitrary operators with respect to the exciton wavefunction,[41,42] which are defined as

$$\langle\hat{O}\rangle_{exc} = \frac{\langle\chi_{exc}|\hat{O}|\chi_{exc}\rangle}{\langle\chi_{exc}|\chi_{exc}\rangle}. \quad (6)$$

An evaluation of exciton properties is straightforward in this framework and standard quantum-chemical methodology can be applied. The denominator in Eq. (6) is the norm of the exciton wavefunction, denoted $\Omega = \langle\chi_{exc}|\chi_{exc}\rangle$, and will reappear in the following discussions. It reflects the single excitation character of an excited state[40] and for normalized wavefunctions its value ranges between 0 and 1 (see also Ref. 48).

2.1 Visualization - *Electron-hole* correlation plots

An instructive way to analyze exciton wavefunctions is to examine the charge-transfer numbers Ω_{AB} (Eq. (5)). For this purpose the system is separated into fragments, and the charge-transfer numbers between them are computed and visualized in a pseudocolor matrix. This so-called *electron-hole* correlation plot provides a coarse-grained representation of the exciton wavefunction, an example of which is shown in Figure 1(c). Local excitation contributions are mapped on the main diagonal going from the lower left to the upper right, while off-diagonal contributions indicate charge transfer between fragments A and B. The relative probability is visualized in grey scale, where black corresponds to the highest probability and white to zero. Although this is a flexible and rather intuitive tool, it has the drawback of requiring an *a priori* definition of the fragmentation. Furthermore, one can expect the same, significant basis-set dependence for Eq. (5) that has been reported for standard Mulliken population analysis, cf. Ref. 49.

2.2 Total charge transfer

In many cases it is desirable to deduce more compact descriptors from the Ω_{AB} matrix[21,43] and in the context of this work it is of particular interest to quantify the total charge transfer. For this purpose, the descriptor

$$\omega_{CT} = \frac{1}{\Omega}\sum_{A}\sum_{B\notin\{A-1,A,A+1\}}\Omega_{AB} \quad (7)$$

is used. As opposed to previous definitions of this descriptor[41,43] only charge transfer between at least second-nearest neighbors is taken into account due to the small sizes of the chosen fragments (see below). ω_{CT} ranges from 0 to 1, where 0 corresponds to a local excitation or Frenkel exciton (with respect to the defined fragmentation scheme) and 1 denotes a completely charge-separated state. Like the underlying Ω_{AB} values, ω_{CT} is sensitive to both, the fragmentation scheme and basis set.

2.3 Functional group contribution

The functional group contribution may be regarded as a specific fragmentation scheme, where the fragments are identified as the functional groups. This is particularly interesting as PPV is composed of two distinct monomer building blocks the phenyl ring (P) and the vinylene group (V). In the fragmentation scheme, we separate the P and V contributions and perform the partial summation

$$\omega_P = \frac{1}{2\Omega}\sum_{P\in\mathscr{P}}\sum_{A}(\Omega_{AP}+\Omega_{PA}) \quad (8)$$

where P runs over the set of phenyl rings $\mathscr{P}$ while A runs over all fragments. ω_P, ranging from 0 to 1, counts the total participation of all phenylene groups to both, *electron* and *hole* of an excitation. Technically, this summation is realized by dividing the system into two formal fragments, one related to all phenyl rings and one to all vinylene groups and counting the excitation contributions that go from and to these fragments.

2.4 Exciton size

Although the charge-transfer numbers Ω_{AB} are a versatile and flexible tool, a simple physical picture is missing in this approach. To eliminate this shortcomming, we recently introduced a formula for the exciton size,[41] i.e. the averaged *electron-hole* separation, as a more tangible quantity. For this purpose, we apply Eq. (6) to the root-mean-square (rms) separation between the *electron* and *hole* positions and define the exciton size as

$$d^2_{exc} = \left\langle (r_h - r_e)^2 \right\rangle_{exc} = \frac{\langle\chi_{exc}|(r_h-r_e)^2|\chi_{exc}\rangle}{\langle\chi_{exc}|\chi_{exc}\rangle} = \frac{1}{\Omega}\iint\gamma^{0I}(r_h,r_e)(r_h-r_e)^2\gamma^{0I}(r_h,r_e)dr_h dr_e. \quad (9)$$

An explicit evaluation of this equation is possible after insertion of Eq. (2) leading to the set of matrix multiplications[41]

$$d^2_{exc} = \frac{1}{\Omega}\sum_{\xi\in\{x,y,z\}}\left(\mathrm{tr}\left(\mathbf{D}^{I0}\mathbf{M}^{(2)}_{\xi}\mathbf{D}^{0I}\mathbf{S}\right) - 2\mathrm{tr}\left(\mathbf{D}^{I0}\mathbf{M}^{(1)}_{\xi}\mathbf{D}^{0I}\mathbf{M}^{(1)}_{\xi}\right) + \mathrm{tr}\left(\mathbf{D}^{I0}\mathbf{S}\mathbf{D}^{0I}\mathbf{M}^{(2)}_{\xi}\right)\right) \quad (10)$$

where $\mathbf{M}^{(k)}_{\xi}$ refers to the multipole matrix of kth order with respect to the Cartesian coordinate ξ, $\mathbf{S}$ is the overlap matrix in the atomic orbital basis and $\mathbf{D}^{I0}$ is the transpose of $\mathbf{D}^{0I}$.

An evaluation of Eq. (10) is straight forward if the 1TDM and multipole matrices are available. However, this information is usually not part of the standard output of quantum-chemical programs and the formula has to be implemented.[41] To allow for an *a posteriori* evaluation, we now derive an approximate version of d_{exc}, which requires only the CT numbers and the coordinates of the nuclei as input. Starting in Eq. (9), the double integral is divided into separate regions pertaining to different atoms M and

N,

$$d_{exc}^2 = \frac{1}{\Omega}\sum_{M,N}\int_M\int_N \gamma^{0I}(r_h,r_e)\underbrace{(r_h-r_e)^2}_{\approx d_{MN}^2}\gamma^{0I}(r_h,r_e)dr_h dr_e. \quad (11)$$

Subsequently, the $(r_h - r_e)^2$ term is approximated by the squared distance between the positions of the respective nuclei d_{MN}^2. The constant term d_{MN}^2 is taken out of the integral

$$d_{exc}^2 \approx \frac{1}{\Omega} d_{MN}^2 \sum_{M,N}\int_M\int_N \gamma^{0I}(r_h,r_e)\gamma^{0I}(r_h,r_e)dr_h dr_e \quad (12)$$

leaving the CT number Ω_{MN} according to Eq. (4). This suggests the definition of an approximate exciton size

$$\widetilde{d}_{exc} = \sqrt{\frac{1}{\Omega}\sum_{M,N}\Omega_{MN}d_{MN}^2}. \quad (13)$$

In contrast to the full implementation, $\widetilde{d}_{exc}$ neglects the spatial extent of the orbitals involved and it is therefore expected that $\widetilde{d}_{exc} \leq d_{exc}$. A detailed evaluation of the accuracy of $\widetilde{d}_{exc}$ can be found in the ESI.†

Although similar equations have been suggested by other researchers,[44,45,50,51] only the present approach is embedded in a clear approximation hierarchy and the formalism is applicable to arbitrary wavefunction models.

2.5 Phenomenological models for exciton wavefunctions

Since high-level *ab initio* methods become prohibitively expensive for large system sizes, it is interesting to test whether the results can be provided with more phenomenological exciton models. While we examine this question only qualitatively at this point, similar methodology can in future be used to evaluate, re-parametrize or adjust existing empirical models allowing for accurate multi-scale descriptions of large systems.

A number of excellent discussions of excitons in polymers is available in literature[11,50,52–54] and we will therefore restrict ourselves to reviewing only the concepts that are immediately relevant to this work. The central idea is to move away from the molecular-orbital picture to the quasi-particle exciton representation. This is achieved mathematically by a coordinate transformation of the exciton wavefunction (Figure 1) into the *electron-hole* separation (or relative) coordinate $r_{he} = r_e - r_h$ and the center-of-mass (CM) coordinate $R = (r_h + r_e)/2$. Furthermore, it is assumed that these two variables are separable and the wavefunction can be rewritten, at least approximately, into a product of the form

$$\chi_{exc}(r_h,r_e) \approx \phi_{sep}(r_{he})\phi_{CM}(R), \quad (14)$$

where ϕ_{sep} describes the intrinsic *electron-hole* wavefunction and ϕ_{CM} the center-of-mass wavefunction. $\phi_{sep}(r_{he})$ describes the relative motions of two oppositely charged particles. Its solutions in a homogeneous medium will therefore possess the same shape as the wavefunctions of a simple hydrogen atom, only that a different effective mass and dielectric susceptibility have to be inserted. By contrast, $\phi_{CM}(R)$ describes a neutral particle, which is not subjected to any Coulomb potential. In a periodic system this yields a plane-wave solution while in a confined molecular system a *particle-in-a-box* picture is adequate, and for more complex branched systems an exciton scattering approach[53] has been developed.

Following the above considerations, we now define the Wannier-Mott picture of excitons in polymers. Here, the radial wavefunctions $\phi_{sep}(r_{he})$ are assumed to resemble hydrogenic s, p, d etc. orbitals only that they extend in a one-dimensional space. These wavefunctions are indexed by a principle quantum number n. Specifically, the exciton size of the Wannier B_u excitons is expected to scale linearly with n according to[19]

$$d_{exc,n} \approx n \times d_{exc,1} \quad (15)$$

where $d_{exc,1}$ is the size for the primary ($n = 1$) exciton. Furthermore, the center-of-mass wavefunctions $\phi_{CM}(R)$ are described by the quasi-momentum quantum number j. These can be identified with *particle-in-a-box*-like wavefunctions possessing $j-1$ nodal planes. In the following text, we will characterize Wannier excitons by the quantum numbers n and j using the notation $W(n,j)$.

The Wannier picture assumes the presence of freely moving quasi-particles. For more localized states the Frenkel exciton model can be applied. This model, whose application to PPV is discussed in detail in Ref. 55, is based on entirely different assumptions: The system is divided into individual sites i, and these give rise to locally excited states $|i\rangle$ that are each confined to the respective site. The excited states of the whole system are obtained as eigenstates of the Hamiltonian

$$\widehat{H}_{Frenkel} = \sum_i \varepsilon_i |i\rangle\langle i| + \sum_{ij} c_{ij}|i\rangle\langle j| \quad (16)$$

where ε_i are the site excitation energies and c_{ij} are the electronic couplings or transfer integrals, which are usually assumed to derive from Coulomb interactions. To understand this equation, it may be helpful to realize that the resulting Hamiltonian matrix $\langle i|\widehat{H}_{Frenkel}|j\rangle$ possesses the same structure as a matrix in Hückel theory, considering only nearest neighbour couplings. Furthermore, considering close-lying ε_i values and small couplings c_{ij}, it is clear that the resulting excitation energies are closely spaced.

3 Computational details

All calculations were performed using variants of the algebraic diagrammatic construction (ADC) scheme for the polarization propagator.[56,57] ADC(2) and ADC(3/2) calculations were performed employing the Q-Chem 4.2 package in a developmental version.[58–61] The abbreviation ADC(3/2) indicates that although excited-state vectors are computed at the third order of perturbation theory, the corresponding densities are computed using these vectors in combination with the second-order intermediate-state basis. For these calculations, an efficient calculation of properties is possible through the intermediate state representation (ISR).[62] For larger systems and basis sets, the Turbomole 6.3.1 program package[63] was used, which affords an efficient implementation of ADC(2) exploiting the resolution-of-the-identity (RI) approximation (RI-ADC(2)).[64–66] The calculations were performed using the Ahlrichs basis sets SV, SV(P), and TZVP[67,68] to examine

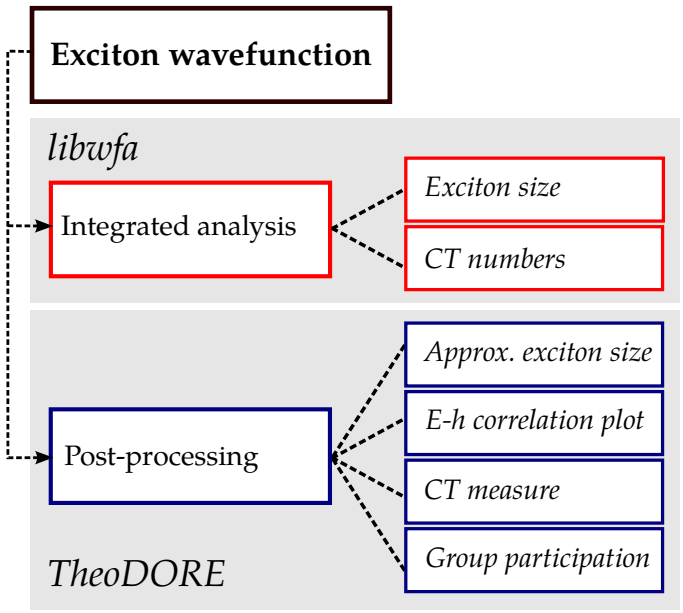

Fig. 2 Wavefunction analysis software used in this work: the libwfa library and the TheoDORE program package.

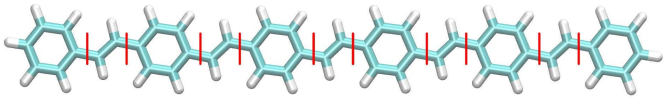

Fig. 3 Fragmentation scheme to compute *electron-hole* correlation plots and ω_{CT} values shown here for $(PV)_5P$.

basis-set effects. For all calculations planar geometries were taken from Ref. 31 and C_{2h} symmetry was used throughout. In the case of the ADC calculations in Q-Chem, the wavefunction analysis library (libwfa)[40–42] was applied to directly analyze the 1TDMs as given by the ISR to compute the exciton size and charge-transfer numbers. This information was, however, not accessible to us in the RI-ADC computations in Turbomole. Therefore the response vectors were read instead and processed externally by the TheoDORE 1.0 analysis package.[69] In all cases, post-processing of the results and the creation of *electron-hole* correlation plots was carried out using TheoDORE.[69] The different software used to compute the various wavefunction properties is summarized in Figure 2. While TheoDORE is publicly available as a stand-alone package, libwfa is distributed as a part of Q-Chem 4.3. The fragmentation scheme used to compute *electron-hole* correlation plots and ω_{CT} numbers is shown in Figure 3. The oligomers were cut into fragments that alternatively represent phenylene rings or vinylene groups yielding, e.g., 11 fragments in the case of $(PV)_5P$.

4 Results and discussion

In this section a detailed analysis of the excited states of poly(*para* phenylene vinylene) oligomers is presented. Firstly, a high-level benchmark of the excitation energies is presented and the role of double excitations is addressed. Secondly, the low-lying excited states of oligomers from two to eight phenyl rings are discussed. These oligomers emulate spectroscopic units, which are usually invoked to explain the properties of the polymer.[3,8,70] In these cases a detailed analysis of the different excited states is carried out. Special attention is devoted to the emergence of exciton bands, which are illustrated by employing pictorial representations, as well as numerical descriptors of the excitations. Thirdly, a large-scale analysis including twenty singlet and twenty triplet excited states of $(PV)_7P$ is performed and the results are interpreted within the exciton models discussed above (Section 2.5).

4.1 High-level benchmark of singly and doubly excited states

The discussion will be started with high-level benchmark calculations performed at the ADC(3) level of theory.[59,71,72] ADC(3) is a polarization-propagator based excited-state method that consistently treats terms to the polarization propagator up to the third order in perturbation theory. It provides a very accurate, third-order description of singly excited states, which are the primary focus of this paper. Also the description of doubly excited states is reasonably accurate and correct to first order of perturbation theory.[60] ADC(2) on the contrary treats all terms at one order of perturbation theory lower than ADC(3) and is therefore not suited to describe doubly excited states. To keep the computational cost at an affordable level, the ADC(3) computations are limited to the smallest three oligomers investigated, i.e. stilbene to $(PV)_3P$.

Vertical excitation energies, oscillator strengths as well as additional excited-state descriptors computed at the ADC(3)/SV(P) level are presented in Table 1 and compared to the analogous ADC(2)/SV(P) results. In this analysis the double excitation character is of particular interest and two different values are used for its quantification. On the one hand, the Ω value, defined as the squared norm of the 1TDM,[40,48] is used providing a universal method-independent measure for single excitation character. On the other hand, the weight of the single excitation amplitudes t_1 is used, which is straightforward to extract from a computation but possesses a meaning only within a chosen computational protocol. Fortunately, as seen in Table 1, the numbers are very similar with the only exception that t_1 is always slightly larger than Ω.

For the smallest oligomer PVP (i.e. stilbene, $n = 1$) the excitation energies of the first three excited states are shifted down by about −0.2 eV when going from ADC(2) to ADC(3). Furthermore, there is a notable transfer of oscillator strength: While the 1^1B_u state is by far the brightest state in the ADC(2) calculation, there is an even distribution of oscillator strength between the 1^1B_u and 2^1B_u states for ADC(3). The remaining values for the first three states shown in Table 1 are rather similar for both methods, and this is also true for the *electron-hole* correlation plots shown in Figure 2 of the ESI.† After these three singly excited states, there are a number of low-energy doubly excited states found with ADC(3), which are missing in the ADC(2) spectrum. A doubly excited state (3^1A_g, $\Omega = 0.19$) is found at 4.66 eV with ADC(3). The excitation energy of this state stands in agreement with both, the experimental value of 4.84 eV, which was predicted by two-photon absorption,[73] and calculations on the CASPT2 level of theory with

Table 1 Vertical excitation energies (ΔE, eV) and oscillator strengths (f) and a selection of excited-state descriptors for $(PV)_nP$ singlet states with $n = 1$ to 3 calculated at the ADC(2)/SV(P) and ADC(3)/SV(P) levels of theory.

	ADC(2)							ADC(3)						
n	state	ΔE	f	Ω	t_1	ω_{CT}	d_{exc}	state	ΔE	f	Ω	t_1	ω_{CT}	d_{exc}
1	1^1B_u	4.543	1.082	0.85	0.91	0.14	4.01	1^1B_u	4.449	0.514	0.80	0.86	0.09	3.61
	2^1A_g	4.844	0	0.83	0.90	0.06	3.33	2^1A_g	4.544	0	0.75	0.81	0.06	3.28
	2^1B_u	4.854	0.089	0.83	0.90	0.08	3.41	2^1B_u	4.629	0.610	0.81	0.87	0.10	3.67
	–							3^1A_g	4.659	0	0.19	0.20	(0.29)	(4.59)
	–							3^1B_u	5.652	0.010	0.23	0.24	(0.04)	(3.88)
	3^1A_g	6.106	0	0.83	0.89	0.24	4.52	5^1A_g	6.108	0	0.82	0.87	0.07	3.51
	–							6^1A_g	6.336	0	0.77	0.81	0.14	3.90
2	–							2^1A_g	3.758	0	0.16	0.17	(0.45)	(6.28)
	1^1B_u	3.814	2.068	0.83	0.90	0.26	5.16	1^1B_u	3.819	1.982	0.83	0.90	0.22	4.81
	2^1B_u	4.526	0.033	0.82	0.89	0.10	3.72	2^1B_u	4.251	0.115	0.74	0.80	0.10	3.70
	2^1A_g	4.780	0	0.83	0.90	0.09	3.72	3^1A_g	4.498	0	0.75	0.81	0.08	3.55
	3^1A_g	4.967	0	0.83	0.89	0.30	5.35	5^1A_g	4.992	0	0.85	0.90	0.14	4.00
3	–							2^1A_g	3.460	0	0.14	0.15	(0.51)	(7.34)
	1^1B_u	3.487	2.959	0.82	0.90	0.32	5.86	1^1B_u	3.504	2.963	0.83	0.90	0.26	5.43
	–							2^1B_u	3.886	0.001	0.16	0.16	(0.45)	(6.32)
	2^1A_g	4.310	0	0.84	0.90	0.23	4.90	3^1A_g	4.184	0	0.75	0.81	0.11	3.92
	2^1B_u	4.495	0.029	0.82	0.89	0.11	3.93	3^1B_u	4.224	0.079	0.74	0.80	0.10	3.84
	3^1A_g	4.516	0	0.82	0.89	0.17	4.57	6^1A_g	4.389	0	0.81	0.87	0.17	4.40

a vertical excitation energy of 4.95 eV.[39] Our analysis protocols of the 1TDM are not applicable to doubly excited states and their character is not discussed further here. However, it should be noted that analysis methods of two-body densities have been indeed introduced in literature.[74–76] By contrast, at the ADC(2) level the 3^1A_g state is located at 6.10 eV and possesses single excitation character. It is the counterpart of the fifth totally symmetric state 5^1A_g at the ADC(3) level. While the amount of single excitation character of this state is the same for both methods, the exciton properties differ significantly. Inspecting the *electron-hole* correlation plot for the 5^1A_g state (see Fig. 2 of ESI) it shows dominant contributions on the phenyl rings but also charge transfer between the rings and towards the vinylene group is present.

Going to the second oligomer $(PV)_2P$, the differences between ADC(2) and ADC(3) are more pronounced: For ADC(3) already the first excited state (2^1A_g) is a dark doubly excited state ($f = 0$, $\Omega = 0.16$). The assumption that this state indeed lies below the bright 1^1B_u state is contradictory to the observation of luminescence in PPV oligomers. However, geometric and environmental effects as well as methodological uncertainty can easily cause a shift by a few tenths of eV which would again establish the bright state as the lowest-energy state. The remaining states are only slightly displaced in energy and the oscillator strengths are almost unaltered. In the case of 1^1B_u a slight lowering of ω_{CT} and d_{exc} is observed for ADC(3) indicating a small reduction in charge-transfer character. Furthermore, the Ω values of the 2^1B_u and 3^1A_g states are lowered to about 0.75, which indicate an enhanced admixture of double excitation character.

In the case of $(PV)_3P$ the lowest excited state at the ADC(3) level is again a doubly excited 2^1A_g state and a doubly excited 2^1B_u state comes into play, as well. By contrast, the bright 1^1B_u state is more or less unaltered with only a small blue shift and a slightly diminished CT character as indicated by ω_{CT} and d_{exc}.

A comparison between the computed results and experimental data is carried out for the 1^1B_u state for oligomers with up to five phenyl rings (cf. Table 2). There are some controversial experimental values from Hohlneicher et al.,[77] Woo et al.[78] and Gierschner et al.,[79] which deviate increasingly as a function of chain length. Our predictions agree very well with the data from Gierschner et al., while previous SAC-CI calculations[33] agree much better with the first series by the other groups. As will be shown below, excitation energies are somewhat lowered with larger basis sets shifting the results more toward Refs. 77,78.

Table 2 Vertical excitation energies (eV) of the first optically allowed 1^1B_u state of $(PV)_nP$ oligomers with $n = 1, ..., 4$.

state	method	$n = 1$	$n = 2$	$n = 3$	$n = 4$
1^1B_u	exp.	4.15[a]	3.50[b]	3.20[b]	3.05[b]
	exp.[c]	4.19	3.69	3.47	3.35
	ADC(2)/SV(P)	4.54	3.81	3.49	3.32
	ADC(3)/SV(P)	4.45	3.82	3.50	-
	SAC-CI/6-31G(d)[d]	4.21	3.57	3.18	3.09

Data taken from [a]Ref. 77, [b] Ref. 78, [c] Ref. 79, [d] Ref. 33.

On the one hand, the presented comparison could certainly demonstrate the accuracy of ADC(2) for these systems as far as energies, oscillator strengths, and wavefunctions of singly excited states are concerned. On the other hand, the ADC(3) computations open a completely new perspective onto low-energy doubly excited states. The presence of such states is not necessarily a surprise, considering their importance for other related systems, e.g. polyenes[80,81] or polyacenes.[82] To our knowledge, however, they have only received little attention so far. It would be of particular interest to explore whether these states have a connection to singlet fission observed in PPV,[83,84] i.e. the generation of two charge carrier pairs from one photon. However, this question has to be postponed to future studies.

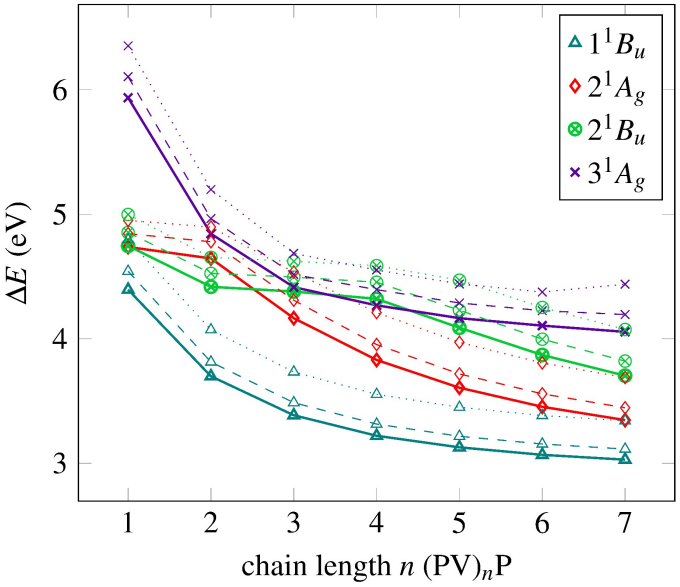

Fig. 4 Vertical excitation energies (ΔE, eV) of poly(*para* phenylene vinylene) oligomers of increasing chain length computed at the RI-ADC(2)/SV (dotted lines), RI-ADC(2)/SV(P) (dashed lines) and RI-ADC(2)/TZVP (solid lines) levels of theory.

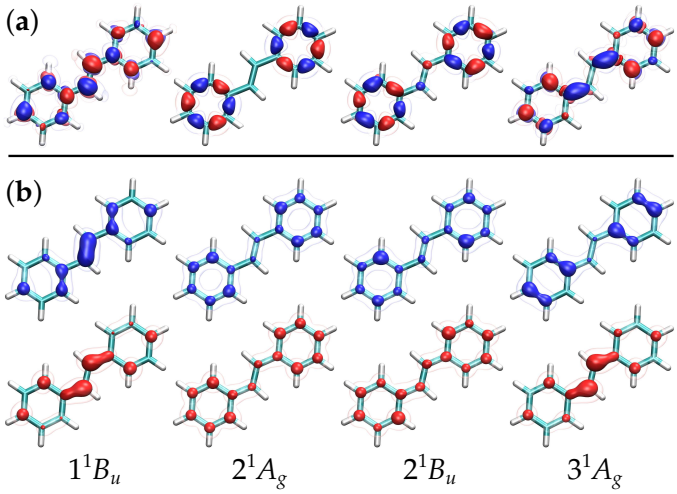

Fig. 5 (a) Transition, (b) *hole* and *electron* densities of first four excited states of stilbene calculated at the ADC(2)/SV(P) level of theory. Isovalues ± 0.003 and ± 0.001, negative (*hole*) densities in blue, positive (*electron*) densities in red.

4.2 Excitons in PPV oligomers of increasing size

Having verified the general suitability of the ADC(2) method for primarily singly excited states, we will now turn to analyzing excited states of PPV oligomers of varying size. The excitation energies of the first four singlet excited states of oligomers with (PV)$_n$P chains from $n = 1$ to 7 are shown in Fig. 4 at the RI-ADC(2) level in combination with three basis sets SV, SV(P) and TZVP. In all cases the lowest excited state is the 1^1B_u state which is significantly lowered in energy for increasing length of the π-conjugated system, e.g. from approximately 4.5 to 3.0 eV in the case of the TZVP basis. This lowering in energy can be rationalized by either considering the diminished gap between the frontier molecular orbitals or by a reduction in kinetic energy[25] deriving from delocalization. For all systems except for the (PV)$_2$P oligomer, the second lowest state is the 2^1A_g and similarly to the 1^1B_u state a significant decrease in excitation energy and a convergence for larger chains is observed. The 2^1B_u energies decrease unsteadily, being similar to the 2^1A_g ones first, and clearly above them for larger oligomers. The highest-energy state in this series is the 3^1A_g state for all oligomers. It starts at $\Delta E = 6.38$ eV for PVP at the TZVP level, shows a significant drop until (PV)$_3$P and stays rather flat for larger systems. The shape of the energy curve is somewhat similar to the 1^1B_u energy curve. Reducing the number of basis functions does not change the qualitative nature of the curves, but systematically raises the excitation energies. The SV(P) curves (dashed lines) lie about $+0.12$ eV higher than the TZVP reference, while the SV curves (dotted lines) are shifted by about $+0.32$ eV. These results stand in agreement with the findings of Ref. 31. We have also examined the first four triplet excited states of the oligomers. The vertical excitation energies are shown in Fig. 3(a) of the ESI.† The triplet states show a completely systematic behaviour throughout the whole oligomer series. The lowest energy state is 1^3B_u followed by the 1^3A_g state. The third state is always the 2^3B_u and the fourth the 2^3A_g state. For all states the excitation energy is significantly lowered in a smooth way with increasing chain length approaching values between 2 and 3 eV. The energy splitting between the lowest triplet and singlet excited state $\Delta E(S_1 - T_1)$ lies between 1.57 eV for PVP and 0.89 eV for (PV)$_7$P which stands in agreement with the findings of Saha et al.[33]

To investigate the characters of the singlet states involved for the different oligomers, we turn to the *electron-hole* correlation plots of the Ω_{AB} matrices (cf. Figure 1(c)). Again the first four singlet excited states of the different oligomers are analyzed and shown in Figure 6. In this figure the excited states are ordered according to their symmetry, which does not necessarily coincide with an arrangement of increasing excitation energies. In the case of the smallest system, stilbene or PVP, the *electron-hole* correlation plots contain a 3 x 3 matrix where the main diagonal goes from the lower left to the upper right. On the main diagonal the first and third element represent the probability for local excitations at the phenyl rings and the central element displays this probability for the vinylene group. Charge transfer between these functional groups is indicated in the respective off-diagonal fields. In the first row going from left to right, the 1^1B_u state is delocalized over the whole PVP molecule and both, charge transfer and local excitation character are present. The 2^1B_u and 2^1A_g states, in contrast, show predominantly local excitation character. The two states represent a pair of excitonic resonance states (see e.g. Ref. 41) consisting of one positive and one negative linear combination of locally excited states at the phenyl rings. The fourth state of this molecule, the 3^1A_g state shows a different excitation pattern compared to the previous ones. Here, local contributions at the phenyl rings are found as well as charge-transfer contributions between each phenyl ring and the vinylene group.

To relate the *electron-hole* correlation plots to more common representations of excited states, the transition densities as well

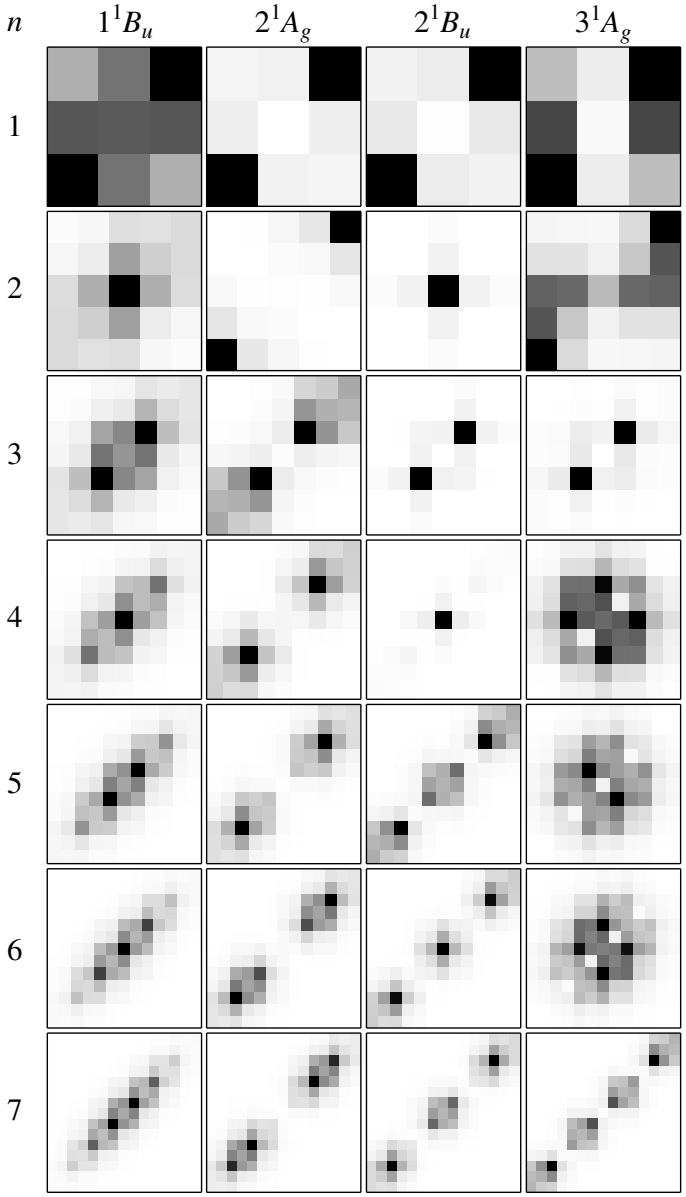

Fig. 6 *Electron-hole* correlation plots of the first four excited states of $(PV)_nP$ oligomers computed at the RI-ADC(2)/TZVP level of theory.

as the *electron* and *hole* densities[40,85] for the four states of stilbene are plotted in Figure 5. The transition density is the diagonal part of the 1TDM, where the *electron* and *hole* are at the same location in space ($r_h = r_e$). This, in turn, means that the main diagonals in the *electron-hole* correlation plots are a coarse representation of the transition densities. Inspecting the plots in Figures 5 and 6, a close correspondence between the different representations can be found. In particular, it is observed that in all cases there are important contributions on the phenyl rings while only the first state (1^1B_u) possesses significant vinylene participation.

The *electron* and *hole* densities correspond to partial summations of the Ω-matrices over individual rows or columns, respectively. Again, a correspondence between the representations can be observed and it is possible to get an impression about the state character. If the *electron* and *hole* densities are rather similar, charge transfer is only involved to a smaller extent (e.g. 2^1A_g and 2^1B_u), while large differences in their spatial distribution indicate a more pronounced charge transfer (e.g. 1^1B_u and 3^1A_g). However, the great advantage of the *electron-hole* correlation plot is that it collects all the presented aspects in one representation, and contains also crucial information about dynamic charge transfer.

Going to the second row in Figure 6, the matrix is increased by one phenylene and one vinylene to 5×5. The first 1^1B_u state is slightly delocalized over the whole system with the dominating contribution on the central phenylene unit. Some charge transfer occurs, mostly between direct and second-nearest neighbours. In contrast, the second and third state of this system have dominantly local nature, concentrated on the terminal and central phenyl rings, respectively. The fourth excited state presented, 3^1A_g, shows enhanced charge-transfer character, where mostly the terminal phenyl rings are involved. The asymmetric pattern with respect to the main diagonal arises from a directed transfer of electron density from the terminal phenyl rings to the inner vinylene and phenylene groups.

In $(PV)_3P$, the first two states are delocalized similar to the 1^1B_u states of the smaller systems and *electron* and *hole* are not separated by more than three functional units. However, a new feature is observed for the 2^1A_g state: A nodal plane perpendicular to the main diagonal is found. This phenomenon, which will appear more prominently for the larger oligomers, is interpreted as a *particle-in-a-box*-like state of higher quasi-momentum. The third and fourth state of the $(PV)_3P$ molecule are again a pair of excitonic resonance states at the central two phenyl rings and the two states are quasi-degenerate.

For the next system $(PV)_4P$, the first two states are, again, delocalized and the third state is a local excitation at the central phenyl ring. Interestingly, for the fourth state, 3^1A_g, a new excitation pattern is found. Here, major CT contributions over larger separations play a dominant role. At the same time, on the main diagonal only three smaller contributions at the phenyl groups around the center take part. This altered intrinsic *electron-hole* structure was earlier assigned to a distinct Wannier exciton band[31,41] and in the above-defined nomenclature this corresponds to a $W(2,1)$ state. In accordance with predictions of Mukamel et al.[36] at this chain length some of the bulk properties

start to become apparent.

Going to larger chains with $n > 4$, the exciton wavefunction patterns reappear and enhanced electronic coherence is present. The very local states are no longer observed for $n \geq 5$ and in the case of $(PV)_7P$ also the charge-separated state disappears and only four similar looking Wannier states, $W(1,j)$ with j between 1 and 4 remain. The other types of states are located at higher relative energies as will be examined in Section 4.3.

While the previous analysis gave an intuitive visual representation of the excited states, we will now proceed to a more compact quantitative analysis. For this purpose the different excited-state descriptors as discussed in Section 2 will be applied to the same set of computations. The exciton sizes ($\widetilde{d}_{exc}$) are presented in Figure 7(a). In case of the 1^1B_u, 2^1A_g and 2^1B_u states these increase steadily with growing system size until they converge against values between 5 and 6 Å. As a common trend, it is observed that the exciton sizes decrease with more nodes perpendicular to the main diagonal as seen in Figure 6, i.e. with a higher translational quantum number j. Contrary to the three lower-energy states, the 3^1A_g states show larger fluctuations in exciton sizes with a minimal value of 4.92 Å for $(PV)_3P$ and a large jump to 9.46 Å for $(PV)_4P$ until the value once again drops to 5.28 Å for $(PV)_7P$. These variations follow the changes in the state character as presented in Figure 6. The charge-separated 3^1A_g states of $W(2,1)$ character found for $n = 4,5,6$ possess large exciton sizes of about 10 Å while the lowering in the case of $n = 7$ coincides with the appearance of the $W(1,4)$ exciton. A more detailed understanding of the variations in state characters could be gained by computing higher excited states, but we will postpone this more elaborate analysis to the next section. An important conclusion of Figure 7(a) is that the exciton size saturates at about 6 Å and does not increase further with increasing system size. A similar trend was found for a variety of polymers in a related study only that a somewhat larger saturation size was found with the chosen computational protocol.[86]

The charge-transfer measures shown in Figure 7(b) are largely consistent with the exciton sizes with some small differences observed only on closer inspection. For example for large oligomers, the three lower energy states 1^1B_u, 2^1A_g and 2^1B_u converge to almost the same value of $\omega_{CT} \approx 0.33$ while a clear separation exists between them with respect to the d_{exc} values. The general consistency between the $\widetilde{d}_{exc}$ and ω_{CT} values facilitates the interpretation of the results by transmitting a clear connection between pictorial representations and quantitative analysis of the exciton wavefunctions. However, the close correspondence between these values shows that in future studies, it may suffice to compute exciton sizes.

As last excited-state descriptor, the functional group contribution as defined in Eq. 8 will be discussed, which is plotted in Figure 7(c). This descriptor accounts for the fraction of excitation that takes place at all phenylene groups of the system, e.g. a high value in ω_P indicates that the excitation mostly occurs at the phenyl rings. In the case of the 1^1B_u states, it is almost constant with values sightly above 0.6. For the other states, the values vary depending on the exciton wavefunction character as examined in the *electron-hole* correlation plots. If the states are

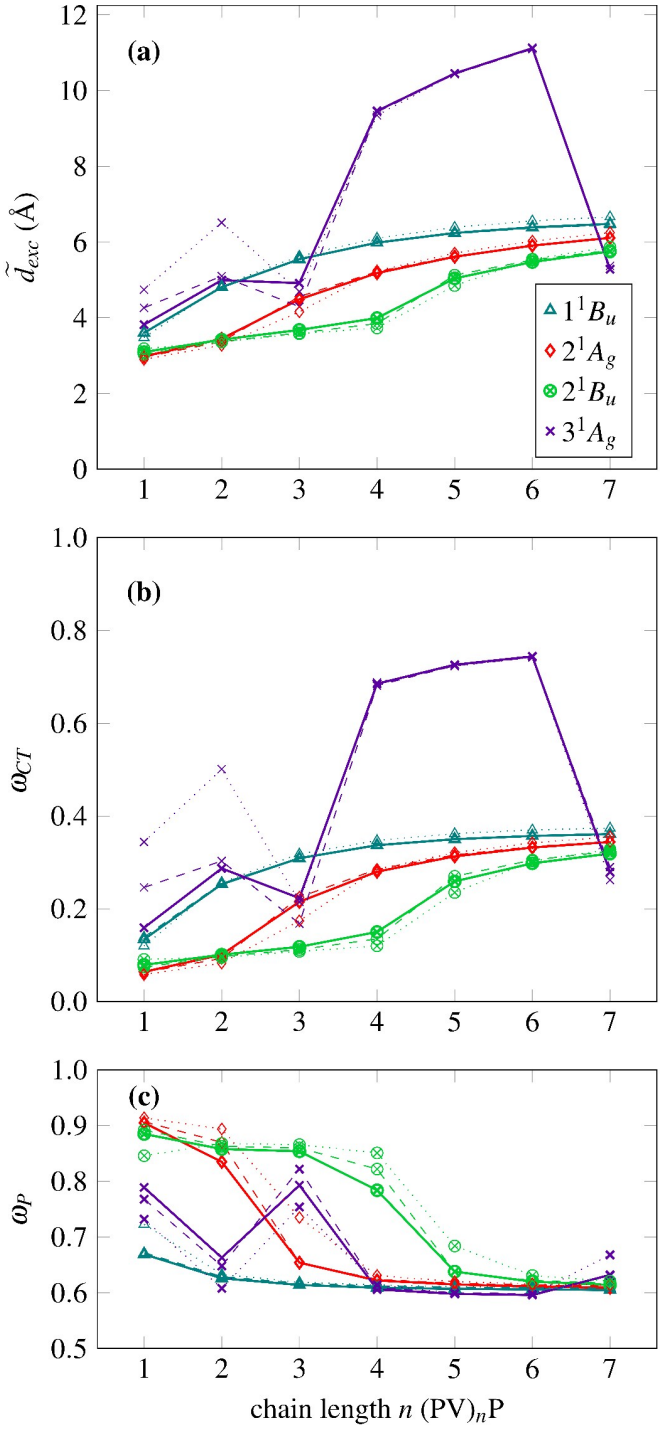

Fig. 7 (a) Approximate exciton sizes ($\widetilde{d}_{exc}$, Å), (b) charge-transfer measures (ω_{CT}) and (c) functional group contribution ω_P of poly(*para* phenylene vinylene) oligomers of increasing chain length computed at the RI-ADC(2)/TZVP (solid lines) RI-ADC(2)/SV(P) (dashed lines) and RI-ADC(2)/SV (dotted lines) levels of theory.

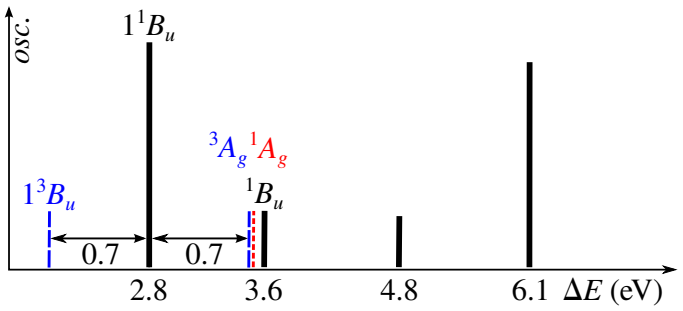

Fig. 8 Schematic excitation spectrum and dark states of PPV deduced from experiment.[87–91] Peaks visible in the absorption spectrum are indicated by solid black lines, dark states are indicated by dashed lines, where red corresponds to singlet and blue to triplet states.

predominantly locally confined at the phenyl rings, they possess high ω_P values ≥ 0.8. However, the values become smaller with increasing chain length indicating that a delocalization over adjacent vinylene groups becomes more important. Interestingly, the charge-transfer 3^1A_g states for $(PV)_nP$ with $n = 5,6$ show the same amount of phenylene contribution as the other exciton states, although we assume them to belong to another band. Summarizing the findings, major differences in ω_P can be associated with Frenkel ($\omega_P \geq 0.8$) or Wannier nature of the states where different Wannier bands exhibit similar behaviour in terms of ω_P.

To estimate basis-set effects on the excited-state descriptors, the values are recalculated at the RI-ADC(2)/SV(P) and RI-ADC(2)/SV levels of theory and the results are shown in Figure 7 as dashed and dotted lines, respectively. The results are largely consistent with the TZVP results for the large oligomers. However for the smallest three oligomers, significant deviations from the TZVP reference are found for the 3^1A_g state hinting on differences in the state character in this special case. For the RI-ADC(2)/SV(P) results the mean absolute error for $\widetilde{d}_{exc}$ is 0.16 Å (mean error −0.09 Å) and for ω_{CT} it amounts 0.01 (mean error 0.00).

Summarizing the results of this section, it was found that for large conjugated systems a band picture emerges featuring different types of excitons, while for smaller oligomers confinement is the dominating effect.

4.3 Systematic study of $(PV)_7P$ excitons

In the previous section, the presence of a number of distinct exciton patterns for the low-lying excited states of different oligomers was revealed. To understand these in more detail, it is necessary to arrange them in a more systematic way. For this purpose, the largest compound presented above, $(PV)_7P$, is chosen and its higher excited states are studied. The first twenty singlet and twenty triplet states are computed at the RI-ADC(2)/TZVP level of theory and analyzed using the methods discussed above. Furthermore, the results are correlated with the phenomenological models discussed in Section 2.5.

To allow for a quick comparison of the findings of this work and experimental results, we will first summarize characteristics of excited states of PPV found by experiment (cf. Figure 8). The absorption spectrum of PPV is dominated by two absorption peaks with high oscillator strength.[87] They lie at 2.8 and 6.1 eV and are polarized parallel to the chain axis. Two weaker absorptions are found at around 3.6 and 4.8 eV, where the prior has a less well-defined polarization but the latter is polarized perpendicular to the chain axis.[87,88] Electroabsorption[87] and two-photon absorption[89] spectroscopy revealed information about three additional states. One dipole-forbidden state can be found at about 0.7 eV above the lowest dipole-allowed state, which is approximately at 3.5 eV. Furthermore there are two triplet states, one lies at approximately 0.7 eV below the lowest bright state[90] and another 0.7 eV above.[91] This latter state is quasi-degenerate to the dipole-forbidden state and these two states are referred to as the singlet and triplet charge-transfer states.[25,92]

An analysis of the computed singlet excited states is presented in Table 3 showing the vertical excitation energies as well as various data about the excited states. The excitation energies range from 3.03 eV up to 5.04 eV with a very dense region of states around 4.3 eV. Only states of B_u symmetry possess non-vanishing oscillator strength due to dipole selection rules. In all these cases the transition moment lies in the molecular plane, pointing along the chain axis. The brightest state with $f = 6.2$ is the 1^1B_u state located at 3.03 eV. This value is somewhat higher than the lowest bright peak in the experimental absorption spectrum with 2.8 eV.[14,87,88,93] The second largest oscillator strength is found for 2^1B_u, which is the $j = 3$ state of the same exciton band. This state could certainly be responsible for the shoulder to the main peak at around 3.7 eV,[87,88] cf. Figure 8. The remaining states have rather small oscillator strengths below 0.25 and could be hidden in the experimental spectrum. The higher energy peaks detected by experiment are most likely beyond the states computed here and, in particular, we find no off-axis polarized state as was reported for the band at 4.7 eV.[88] The 10^1B_u state at 4.87 eV, which is the $W(3,1)$ exciton, matches from an energetic viewpoint but due to its rather small oscillator strength of 0.224 and its polarization along the main axis we do not assign it to the experimental peak. The experimentally characterized, dipole-forbidden state can be identified as the 4^1A_g at 4.07 eV, which is blue-shifted compared to the experimental value of ≈ 3.5 eV.

In the case of the triplet states the data is summarized in Table 4. Here, excitation energies are shifted to smaller values compared to the singlets and range from 2.12 eV up to 4.59 eV. Like in the case of the singlets there is a dense region of states around 4.3 eV. The two triplet states that have been reported from experiment can both be identified with calculated states: The lowest-energy triplet 1^3B_u state lies at 2.12 eV which stands in agreement with the measured value of 2.1 eV. Moreover, the second state with an excitation energy of 4.17 eV is the 5^3A_g state, which is again blue-shifted w.r.t. experiment by about 0.7 eV. The 4^1A_g and 5^3A_g states are quasi-degenerate as expected as they both belong to the $n = 2$ branch of Wannier excitons. As we will see later in the *electron-hole* correlation plots, they have odd-parity wavefunctions with respect to the *electron-hole* separation coordinate. This pair of states is referred to as the singlet-triplet charge-transfer states and are proposed to play an important role in the formation of free charge carriers.[25] Comparing excitation ener-

Table 3 Vertical excitation energies (ΔE, eV), oscillator strengths (f), weight of the single excitation amplitudes (t_1), charge transfer (ω_{CT}), exciton size ($\widetilde{d}_{exc}$), phenyl group participation (ω_P), and type assignments computed for $(PV)_7P$ singlet excited states at the RI-ADC(2)/TZVP level of theory.

	state	ΔE	f^*	t_1	ω_{CT}	$\widetilde{d}_{exc}$	ω_P	type†
1	1^1B_u	3.028	6.212	0.93	0.36	6.48	0.61	$W(1,1)$
2	2^1A_g	3.346	0	0.93	0.34	6.11	0.61	$W(1,2)$
3	2^1B_u	3.703	0.654	0.93	0.32	5.75	0.61	$W(1,3)$
4	3^1A_g	4.055	0	0.93	0.28	5.28	0.63	$W(1,4)$
5	4^1A_g	4.070	0	0.90	0.75	11.59	0.60	$W(2,1)$
6	3^1B_u	4.254	0.000	0.90	0.69	10.01	0.61	$W(2,2)$
7	4^1B_u	4.309	0.101	0.92	0.16	4.16	0.78	F
8	5^1B_u	4.344	0.033	0.91	0.15	4.39	0.84	F
9	5^1A_g	4.356	0	0.91	0.14	4.10	0.84	F
10	6^1A_g	4.361	0	0.91	0.14	4.08	0.84	F
11	6^1B_u	4.390	0.026	0.91	0.15	4.29	0.84	F
12	7^1A_g	4.399	0	0.91	0.17	4.46	0.83	F
13	7^1B_u	4.498	0.173	0.92	0.23	4.82	0.70	$W(1,5)$
14	8^1A_g	4.511	0	0.90	0.63	8.89	0.62	$W(2,3)$
15	9^1A_g	4.670	0	0.92	0.11	3.68	0.86	F
16	8^1B_u	4.688	0.013	0.92	0.13	3.92	0.87	F
17	9^1B_u	4.771	0.005	0.90	0.62	8.19	0.61	$W(2,4)$
18	10^1A_g	4.829	0	0.93	0.23	4.67	0.66	$W(1,6)$
19	10^1B_u	4.866	0.224	0.90	0.88	20.73	0.60	$W(3,1)$
20	11^1A_g	5.037	0	0.89	0.60	7.56	0.58	$W(2,5)$

*All bright states shown are polarized along the chain axis.
†Assignment as Wannier exciton $W(n,j)$ or Frenkel exciton F, see Section 2.5.

Table 4 Vertical excitation energies (ΔE, eV), weight of the single excitation amplitudes (t_1), charge transfer (ω_{CT}), exciton size ($\widetilde{d}_{exc}$), phenylene group participation (ω_P), and type assignments computed for $(PV)_7P$ triplet excited states at the RI-ADC(2)/TZVP level of theory.

	state	ΔE	t_1	ω_{CT}	$\widetilde{d}_{exc}$	ω_P	type*
1	1^3B_u	2.123	0.98	0.22	4.98	0.55	$W(1,1)$
2	1^3A_g	2.248	0.98	0.20	4.63	0.55	$W(1,2)$
3	2^3B_u	2.429	0.98	0.17	4.25	0.55	$W(1,3)$
4	2^3A_g	2.652	0.98	0.14	3.90	0.54	$W(1,4)$
5	3^3B_u	2.903	0.98	0.12	3.57	0.53	$W(1,5)$
6	3^3A_g	3.166	0.98	0.09	3.26	0.50	$W(1,6)$
7	4^3B_u	3.418	0.98	0.07	3.00	0.42	$W(1,7)$
8	4^3A_g	3.869	0.98	0.05	2.98	0.83	$W(1,8)$
9	5^3B_u	4.070	0.98	0.03	2.68	0.74	$W(1,9)$
10	5^3A_g	4.174	0.96	0.82	13.17	0.60	$W(2,1)$
11	6^3A_g	4.268	0.98	0.06	3.00	0.77	$W(1,10)$
12	6^3B_u	4.282	0.97	0.15	4.51	0.85	F
13	7^3A_g	4.296	0.98	0.13	4.18	0.86	F
14	7^3B_u	4.301	0.97	0.15	4.39	0.85	F
15	8^3B_u	4.348	0.98	0.14	4.30	0.85	F
16	8^3A_g	4.351	0.98	0.10	3.59	0.86	F
17	9^3A_g	4.371	0.98	0.09	3.48	0.80	F
18	9^3B_u	4.389	0.96	0.71	10.88	0.63	$W(2,2)$
19	10^3B_u	4.504	0.99	0.03	2.51	0.75	F
20	10^3A_g	4.594	0.98	0.22	5.67	0.80	F

*Assignment as Wannier exciton $W(n,j)$ or Frenkel exciton F, see Section 2.5.

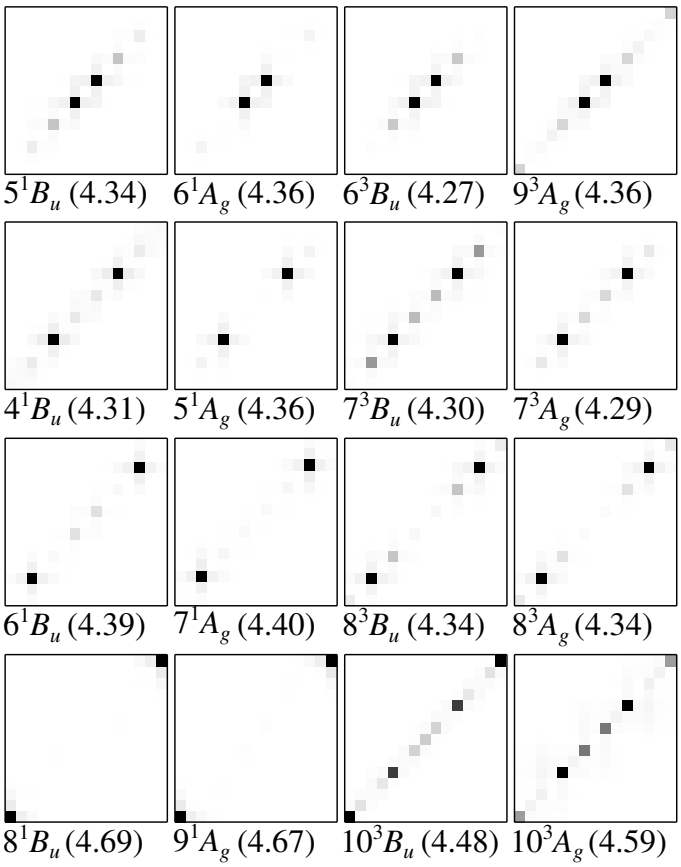

Fig. 9 *Electron-hole* correlation plots of the singlet and triplet Frenkel-type excitonic states for $(PV)_7P$ (excitation energies in eV in parentheses).

gies of the lowest-lying singlet and triplet states, a gap of 0.91 eV is found similar to values that have been reported for this gap at the polymer limit.[94]

In a next step we present pictorial representations of the different excited states. For this purpose, the states are divided into local and delocalized states, or in other words Frenkel and Wannier excitons, based on the information in Tables 3 and 4. Frenkel excitons are distinguished by small exciton sizes and charge transfer combined with enhanced participation of the phenyl rings. In the case of $(PV)_7P$, eight local states of this type should be present, one for each phenyl ring. Inspecting the singlet excited states these can be identified as the states possessing $\omega_{CT} < 0.23$, $\widetilde{d}_{exc} < 4.50$ Å, and $\omega_P > 0.75$. The situation is less clear in the triplet case as there is some mixing between the Frenkel and the more compact Wannier states, but nevertheless eight states were identified as Frenkel excitons (these are marked *F* in Table 4). The *electron-hole* correlation plots for the singlet and triplet Frenkel excitons are presented in Figure 9. Due to the C_{2h} symmetry of the system, the excitations are always distributed over pairs of rings separated by an equal distance from the center of the molecule. In Figure 9 these are arranged by showing the states with excitations on the central phenyl rings on top and moving to the outer part below. The excitation patterns and excitation energies are similar between the singlet and triplet states. This agreement supports the idea that the interactions are dominated by Coulomb coupling, which acts independently of the spin. A determination of the couplings [c_{ij} in (16)] is not straightforward in this complex system, but a glance at the energy scale shows that these are probably not much larger than 0.01 eV. As a final note, it should be pointed out that these states lie significantly below the bright band at 6 eV that is usually assigned Frenkel character.[21,88,93] A comparison to these higher-lying Frenkel states could be of interest but is out of the scope of this investigation.

The structures of the delocalized Wannier excitons are more complicated and, as explained in Section 2.5, it is favorable to discriminate between two independent phenomena: (*i*) the intrinsic structure of the *electron-hole* pair, which is determined by the relative motions of the *electron* and *hole*, and (*ii*) the combined exciton quasi-particle. For this purpose, we adopt a two-index nomenclature $W(n,j)$ where n is the quantum number of the intrinsic wavefunction and j indicates the quasi-momentum of the *particle-in-a-box*-like state. The intrinsic quantum number correlates with the number of nodal planes in parallel to the main diagonal (going from lower left to upper right). Each of these main types gives rise to a series of *particle-in-a-box*-like states with different j, which are in turn characterized by the number of nodal planes perpendicular to the main diagonal.

The discussion is started with the singlet excitons shown in Figure 10 (top). In this case examples for n ranging from 1 to 3 were obtained within the first twenty states. Six $W(1,j)$ excitons starting at 3.03 eV can be found while the $W(2,j)$ series starts at 4.07 eV and consists of five states in the examined energy range. Besides these, there is one $W(3,j)$ exciton at 4.87 eV. The idealized $W(2,j)$ wavefunctions possess odd-parity with respect to the *electron-hole* separation. Accordingly, the probability of the *electron* and *hole* occupying the same position tends toward zero, which in turn means that the transition density vanishes everywhere in space and that the Ω_{AA} elements vanish almost completely. As a consequence of the vanishing transition density,[40] none of these states possesses any noticeable oscillator strength.[21] By contrast, all the $W(1,j)$ and $W(3,j)$ excitons of B_u symmetry exhibit oscillator strengths above 0.15. In the case of the triplet Wannier-type excitons, only two series are encountered within the first twenty states, $W(1,j)$ and $W(2,j)$. The $W(1,j)$ series starts at 2.13 eV and consists of ten states. In this series the lower-energy states present the clear *particle-in-a-box*-like picture found in the singlet case while the higher-energy states possess reduced CT character and start to resemble the Frenkel states. The fact that these triplet states are positioned at lower energy and possess reduced charge-transfer character when compared to the singlets stands in agreement with the expected effects of missing exchange repulsion.[19] In contrast to the $W(1,j)$ excitons the triplet $W(2,j)$ series starts at 4.17 eV and rather resembles the properties of the singlet case (with the exception that only two states of this type were computed here).

After the visual classification of the state characters, a quantitative analysis is performed to further refine the description of the states. For this purpose, the exciton sizes $\widetilde{d}_{exc}$, charge-transfer measures ω_{CT} and functional group participation ω_P of the various singlet and triplet states are plotted against the excitation energies in Figure 11. The Frenkel excitons are found clustered

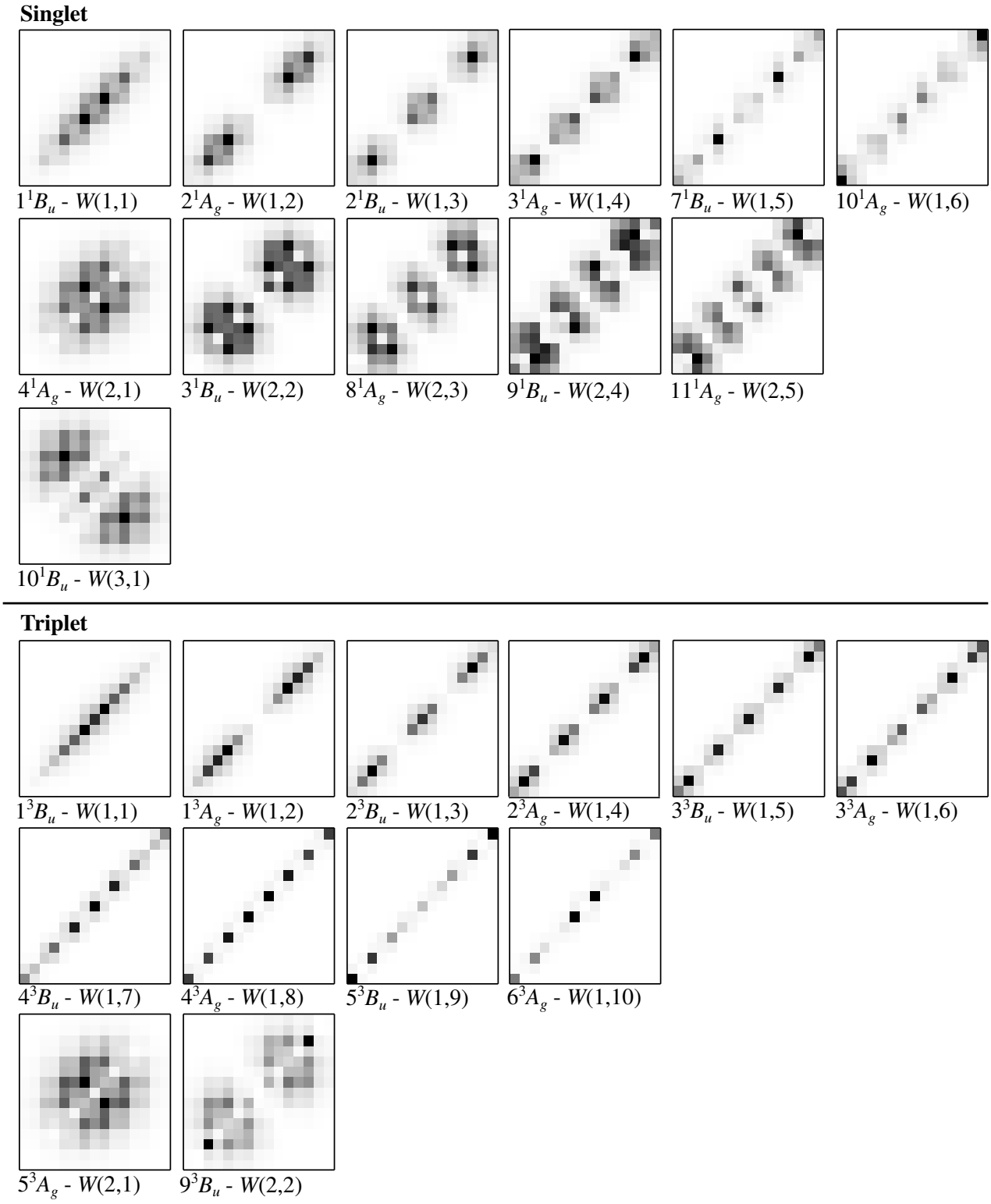

Fig. 10 *Electron-hole* correlation plots of Wannier-type singlet and triplet excitons of $(PV)_7P$, as well as, assignment of principle n and *center-of-mass* quantum numbers j, written $W(n,j)$.

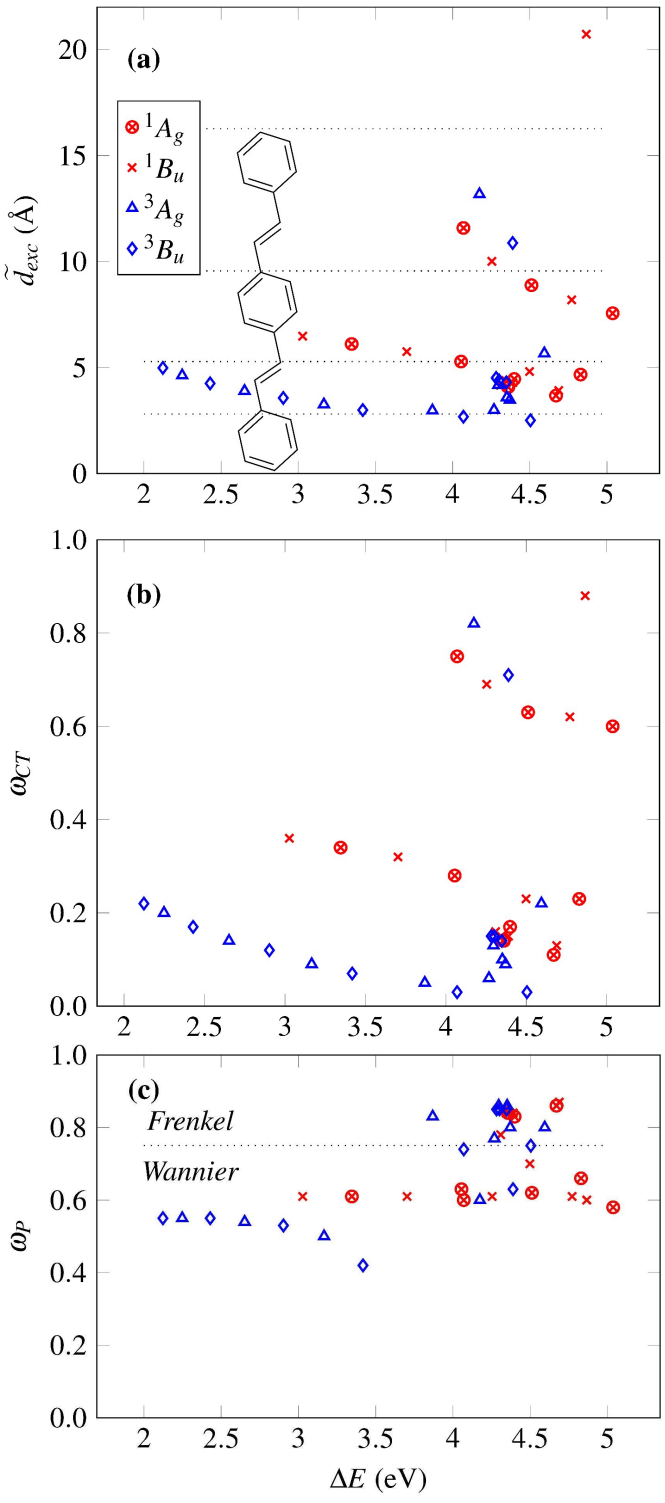

Fig. 11 Analysis of excited states of $(PV)_7P$: (a) Exciton sizes $\widetilde{d}_{exc}$, (b) charge-transfer measures ω_{CT}, and (c) functional group participation ω_P of singlet and triplet excitons plotted against vertical excitation energy at the RI-ADC(2)/TZVP level of theory. The inset in (a) shows the size of a PPV oligomer for comparison.

around an excitation energy of about 4.3 eV. They are characterized by small ω_{CT} values (below 0.23) and exciton sizes ranging between 2.51 and 4.51 Å. Comparing these values to molecular and fragment sizes, they lie between the size of an individual phenyl ring and a PV subunit, both indicated by dotted lines in Figure 11(a). Charge-transfer measures of the Frenkel states are below 0.23 for all states resembling the ω_{CT} values of locally confined excitations in the oligomer series in Sec. 4.2. The Wannier excitons present a different picture showing a large dispersion of the excitation energies with varying quasi-momentum and strong variations in the $\widetilde{d}_{exc}$ and ω_{CT} measures. Different series of data points are, however, clearly apparent and a more detailed examination shows that they indeed correspond to the previously defined exciton types. For the singlet $W(1,j)$ series marked in red, $[\mathrm{x},\otimes]$ in Figure 11, exciton sizes start at 6.48 Å, which is somewhat larger than a PV subunit, slowly decreasing towards 4.67 Å. The corresponding charge-transfer measures lie between 0.36 and 0.23. In contrast, the $W(2,j)$ series starts at exciton sizes of 11.59 Å, about the size of a PVPV fragment, decreasing to 7.56 Å. The $W(2,1)$ exciton is almost double the size of $W(1,1)$, in agreement with Eq. (15).[19] In Figure 11 (a) there is an isolated data point at $\widetilde{d}_{exc} = 20.73$ Å. It belongs to the $W(3,1)$ exciton, which also possesses the large ω_{CT} value of 0.88. The triplet excitons are marked in blue $[\diamond,\triangle]$ in Fig. 11. The $W(1,j)$ series starts slightly above 2 eV with the $W(1,1)$ exciton possessing an exciton size of 4.98 Å. The series slowly decreases towards a size of 3.00 Å. The second triplet exciton series $W(2,j)$ starts at exciton sizes more than twice as large as the $W(1,j)$ excitons with 13.17 Å and contains a second state at 10.88 Å. A general trend found in Figure 11 is that excitons become more tightly bound with increasing quasi-momentum (see also Ref. 44). This shows that the intrinsic wavefunction is not completely separated from the combined quasi-particle motion. It will certainly be of interest to determine whether similar effects are found for other systems.

In band models three different types of excitons are usually considered to be responsible for the excitation spectrum of PPV. These are constructed from two different types of bands, one has delocalized orbital contributions over phenylene and vinylene groups (d and d^*) and one has localized orbitals confined at the phenyl rings with zero orbital contributions at the bridging C-atoms connected to the vinylene groups (l and l^*). The first exciton is a Wannier-type exciton with a transition between delocalized bands ($d \rightarrow d^*$), the second is an intermediate species with transitions between different band types ($l \rightarrow d^*$ and $d \rightarrow l^*$) and the third is a Frenkel-type exciton with a transition between localized bands ($l \rightarrow l^*$).[19,21] In the present quantum-chemical framework, the contributing molecular orbitals are computed without *a priori* assumptions and therefore it is interesting to examine the participation of the two functional groups to different excitonic states identified earlier. For this purpose, we use the ω_P value defined in Eq. 8, which counts the probability of *electron* or *hole* to be found at a phenyl ring plotted in Figure 11(c). The results show that Wannier excitons are in general composed of an even mixture of phenylene and vinylene orbital contributions with ω_P values ranging between 0.42 and 0.66. For example the 1^1B_u state has an ω_P value of 0.61 and the 1^3B_u state a somewhat

smaller value of 0.55. This observation is truly independent from the quantum numbers n or j. This stands in good agreement with the picture of delocalized bands responsible for the $d \rightarrow d^*$ transitions. In contrast, Frenkel states show much larger ω_P values of ≈ 0.85 indicating that these are primarily localized on the phenylene groups. However, it should be noted that there are indeed resonances with the vinylene groups, which contribute about 15% of the excitation. The delocalization effect may in fact be responsible for the small excitation energies of these states compared to isolated benzene rings. In the whole set of excited states we do not find any states with more than 50% vinylene contribution. In fact, the states with large vinylene group contributions are always at least delocalized over the adjacent phenylene carbon atoms.

5 Conclusions

In this work, we presented high-level *ab initio* calculations of the excited states of poly(*para* phenylene vinylene) oligomers and interpreted them using specialized wavefunction analysis protocols. The results showed a good agreement with experimental findings and essential excitonic properties were reproduced. Furthermore, a variety of details about the exciton wavefunctions could be elucidated in qualitative and quantitative analyses.

High-level benchmark computations employing the ADC(3) method were presented for the smallest three oligomers. Aside from verifying the accuracy of the ADC(2) method with respect to energies, oscillator strengths, and wavefunctions of primarily singly excited states, this examination highlighted the importance of low-energy doubly excited states. These have received little attention so far, but we want to point out that they represent ideal doorway states for singlet fission, as observed in PPV.[83,84]

The influence of increasing the size of the π conjugated system on the excited states was investigated. For this purpose, a set of eight oligomers was constructed ranging from two to eight phenyl rings. While for the smaller oligomers, confinement effects dominated, delocalization and the formation of exciton bands was observed for the larger cases. These changes were illustrated in a pictorial representation, using *electron-hole* correlation plots, as well as quantified through excited-state descriptors.

The largest compound, $(PV)_7P$, was analyzed in detail investigating the first twenty singlet and twenty triplet excited states. A detailed examination of exciton wavefunctions revealed the presence of different exciton bands which were identified as Wannier or Frenkel excitons. For Wannier excitons, bands of varying quasi-momentum were identified. A comparison of singlet and triplet excitons revealed that the latter exhibited more tightly bound *electron-hole* pairs leading to significantly lower excitation energies which matches experimental findings. A characterization in terms of the participation of the phenylene and vinylene functional groups was provided. The results of this study highlighted some new aspects, which were previously not at the center of attention, pertaining to (i) the systematic lowering of *electron-hole* separation distances with increasing quasi-momentum for Wannier excitons, (ii) the importance of low-energy doubly excited states, and (iii) the presence of a band of dark low-energy Frenkel excitons around 4.5 eV. Understanding these points and determining whether (i) and (ii) are general phenomena in conjugated organic polymers will require extended studies in future. Furthermore, it will be beneficial to examine the effects of structural fluctuations and of dielectric screening, which is expected to be strong and variable in bulk PPV.[19] These questions will be addressed in forthcoming work employing ADC in combination with equilibrium and non-equilibrium polarizable continuum models[95] and appropriate structural sampling.

Acknowledgement

We dedicate this work to our beloved colleague and friend Michael Wormit in grateful memory. S.A.M. and J.M.M. acknowledge funding from Heidelberg Graduate School of Mathematical and Computational Methods for the Sciences and S.A.M. from the Landesgraduiertenförderung Baden-Württemberg. F.P. has been a fellow of the Alexander von Humboldt-Stiftung and is currently supported by the research school of the Vienna Scientific Cluster. Discussions with I. Burghardt and H. Lischka during the earlier stages of this project are gratefully acknowledged. The authors thank T. R. Plasser for inspiration.

References

1 J.-L. Bredas, J. Cornil and A. J. Heeger, *Adv. Mater.*, 1996, **8**, 447–452.
2 A. J. Heeger, *Angew. Chem. Int. Ed.*, 2001, **40**, 2591–2611.
3 J. Gierschner, J. Cornil and H.-J. Egelhaaf, *Adv. Mater.*, 2007, **19**, 173–191.
4 E. Collini and G. D. Scholes, *Science*, 2009, **323**, 369–373.
5 T. M. Clarke and J. R. Durrant, *Chem. Rev.*, 2010, **110**, 6736–6767.
6 A. O. Patil, A. J. Heeger and F. Wudl, *Chem. Rev.*, 1988, **88**, 183–200.
7 J.-L. Bredas, J. Cornil, D. Beljonne, D. A. Dos Santos and Z. Shuai, *Acc. Chem. Res.*, 1999, **32**, 267–276.
8 G. D. Scholes and G. Rumbles, *Nature Materials*, 2006, **5**, 683–696.
9 I. G. Scheblykin, A. Yartsev, T. Pullerits, V. Gulbinas and V. Sundström, *J. Phys. Chem. B*, 2007, **111**, 6303–6321.
10 W. J. D. Beenken, *Phys. Status Solidi A*, 2009, **206**, 2750–2756.
11 S. Brazovskii and N. Kirova, *Chem. Soc. Rev.*, 2010, **39**, 2453–2465.
12 M. Kuik, G.-J. A. H. Wetzelaer, H. T. Nicolai, N. I. Craciun, D. M. De Leeuw and P. W. M. Blom, *Adv. Mater.*, 2014, **26**, 512–531.
13 L. H. Campbell, T. W. Hagler, D. L. Smith and J. P. Ferraris, *Phys. Rev. Lett.*, 1996, **76**, 1900–1903.
14 M. Liess, S. Jeglinski and Z. V. Vardeny, *Phys. Rev. B*, 1997, **56**, 15712–15723.
15 P. Gomes da Costa and E. M. Conwell, *Phys. Rev. B*, 1993, **48**, 1993–1996.
16 R. Kersting, U. Lemmer, H. J. Bakker, R. F. Mahrt, H. Kurz, V. I. Arkhipov, H. Bässler and E. O. Göbel, *Phys. Rev. Lett.*, 1994, **73**, 1440–1443.
17 D. Moses, J. Wang, A. J. Heeger, A. Kirova and S. Brazovski,

Proc. Nat. Acad. Sci., 2001, **98**, 13413500.
18 T. G. Pedersen, P. M. Johansen and H. C. Pedersen, *Phys. Rev. B*, 2000, **61**, 10504–10510.
19 N. Kirova, *Polym. Int.*, 2008, **57**, 678–688.
20 D. Beljonne, Z. Shuai, R. H. Friend and J.-L. Bredas, *J. Chem. Phys.*, 1995, **102**, 2042.
21 S. Tretiak and S. Mukamel, *Chem. Rev.*, 2002, **102**, 3171–3212.
22 C. De Leener, E. Hennebicq, J.-C. Sancho-Garcia and D. Beljonne, *J. Phys. Chem. B*, 2009, **113**, 1311–1322.
23 V. Lukeš, R. Šolc, M. Barbatti, H. Lischka and H.-F. Kauffmann, *J. Theor. Comput. Chem.*, 2010, **09**, 249–263.
24 M. Y. Lavrentiev, W. Barford, S. J. Martin and D. H., *Phys. Rev. B*, 1999, **59**, 9987–9994.
25 R. J. Bursill and W. Barford, *J. Chem. Phys.*, 2009, **130**, 234302.
26 A. Pogantsch, G. Heimel and E. Zojer, *J. Chem. Phys.*, 2002, **117**, 5921.
27 S. Tretiak, K. Igumenshchev and V. Chernyak, *Phys. Rev. B*, 2005, **71**, 033201.
28 H. Ma, T. Qin and A. Troisi, *J. Chem. Theory Comp.*, 2014, **10**, 1272–1282.
29 M. Rohlfing and S. G. Louie, *Phys. Rev. Lett.*, 1999, **82**, 1959–1962.
30 J.-W. van der Horst, P. A. Bobbert, M. A. J. Michels and H. Bässler, *J. Chem. Phys.*, 2001, **114**, 6950.
31 A. N. Panda, F. Plasser, A. J. A. Aquino, I. Burghardt and H. Lischka, *J. Phys. Chem. A*, 2013, **117**, 2181–2189.
32 T. M. Cardozo, A. J. A. Aquino, M. Barbatti, I. Borges and H. Lischka, *J. Phys. Chem. A*, 2015, **119**, 1787–1795.
33 B. Saha, M. Ehara and H. Nakatsuji, *J. Phys. Chem. A*, 2007, **111**, 5473–5481.
34 T. Nelson, S. Fernandez-Alberti, V. Chernyak, A. E. Roitberg and S. Tretiak, *J. Phys. Chem. B*, 2011, **115**, 5402–5414.
35 R. Binder, J. Wahl, S. Römer and I. Burghardt, *Faraday Discussions*, 2013, **163**, 205.
36 S. Mukamel, S. Tretiak, T. Wagersreiter and V. Chernyak, *Science*, 1997, **277**, 781–787.
37 S. A. Mewes, F. Plasser and A. Dreuw, *J. Chem. Phys.*, 2015, **143**, 171101.
38 J. Quenneville and T. J. Martínez, *J. Phys. Chem. A*, 2003, **107**, 829–837.
39 V. Molina, M. Merchán and B. O. Roos, *J. Phys. Chem. A*, 1997, **101**, 3478–3487.
40 F. Plasser, M. Wormit and A. Dreuw, *J. Chem. Phys.*, 2014, **141**, 024106.
41 S. A. Bäppler, F. Plasser, M. Wormit and A. Dreuw, *Phys. Rev. A*, 2014, **90**, 052521.
42 F. Plasser, B. Thomitzni, S. A. Bäppler, J. Wenzel, D. R. Rehn, M. Wormit and A. Dreuw, *J. Comp. Chem.*, 2015, **36**, 1609–1620.
43 F. Plasser and H. Lischka, *J. Chem. Theory Comp.*, 2012, **8**, 2777–2789.
44 A. V. Luzanov, *J. Struct. Chem.*, 2002, **43**, 711–720.
45 J. Rissler, *Chem. Phys. Lett.*, 2004, **395**, 92–96.
46 A. L. L. East and E. C. Lim, *J. Chem. Phys.*, 2000, **113**, 8981–8994.
47 A. V. Luzanov and O. A. Zhikol, *Int. J. Quant. Chem.*, 2010, **110**, 902–924.
48 S. Matsika, X. Feng, A. V. Luzanov and A. I. Krylov, *J. Phys. Chem. A*, 2014, **118**, 11943–11955.
49 A. E. Reed, R. B. Weinstock and F. Weinhold, *J. Chem. Phys.*, 1985, **82**, 735–746.
50 W. Barford and N. Paiboonvorachat, *J. Chem. Phys.*, 2008, **129**, 162716.
51 H. Ma, T. Qin and A. Troisi, *J, Chem. Theory Comput.*, 2014, **10**, 1272–1282.
52 W. Barford, *J. Phys. Chem. A*, 2013, **117**, 2665–2671.
53 C. Wu, S. V. Malinin, S. Tretiak and V. Y. Chernyak, *J. Chem. Phys.*, 2008, **129**, 174111.
54 D. Abramavicius, B. Palmieri, D. V. Voronine, F. Sanda and S. Mukamel, *Chem. Rev.*, 2009, **109**, 2350–2408.
55 R. Binder, S. Römer, J. Wahl and I. Burghardt, *J. Chem. Phys.*, 2014, **141**, 014101.
56 J. Schirmer, *Phys. Rev. A*, 1982, **26**, 2395–2416.
57 A. B. Trofimov and J. Schirmer, *J. Phys. B*, 1995, **28**, 2299–2324.
58 M. Wormit, D. R. Rehn, P. H. Harbach, J. Wenzel, C. M. Krauter, E. Epifanovsky and A. Dreuw, *Mol. Phys.*, 2014, **112**, 774–784.
59 P. H. P. Harbach, M. Wormit and A. Dreuw, *J. Chem. Phys.*, 2014, **141**, 064113.
60 A. Dreuw and M. Wormit, *WIREs Comput. Mol. Sci.*, 2015, **5**, 82–95.
61 Y. Shao, L. F. Molnar, Y. Jung, J. Kussmann, C. Ochsenfeld, S. T. Brown, A. T. Gilbert, L. V. Slipchenko, S. V. Levchenko, O. D. P., R. A. DiStasio Jr, R. C. Lochan, T. Wang, G. J. Beran, N. A. Besley, J. M. Herbert, C. Yeh Lin, T. Van Voorhis, S. Hung Chien, A. Sodt, R. P. Steele, V. A. Rassolov, P. E. Malsen, P. P. Korambath, R. D. Adamson, B. Austin, J. Baker, E. F. C. Byrd, H. Dachsel, R. J. Doerksen, A. Dreuw, B. D. Dunietz, A. D. Dutoi, T. R. Furlani, S. R. Gwaltney, A. Heyden, S. Hirata, C.-P. Hsu, G. Kedziora, R. Z. Khalliulin, P. Klunzinger, A. M. Lee, W. Liang, I. Lotan, N. Nair, B. Peters, E. I. Proynov, P. A. Pieniazek, Y. Min Rhee, J. Ritchie, E. Rosta, C. David Sherrill, A. C. Simmonett, J. E. Subotnik, H. Lee Woodcock III, W. Zhang, A. T. Bell, A. K. Chakraborty, D. M. Chipman, F. J. Keil, A. Warshel, W. J. Hehre, H. F. Schaefer III, J. Kong, A. I. Krylov, M. Gill, Peter and M. Head-Gordon, *Phys. Chem. Chem. Phys.*, 2006, **8**, 3172.
62 J. Schirmer, *Phys. Rev. A*, 1991, **43**, 4647–4659.
63 *TURBOMOLE V6.4 2012, a development of University of Karlsruhe and Forschungszentrum Karlsruhe GmbH, 1989-2007, TURBOMOLE GmbH, since 2007; available from* `http://www.turbomole.com`.
64 C. Hättig and F. Weigend, *J. Chem. Phys.*, 2000, **113**, 5154–5161.

65 C. Hättig and K. Hald, *Phys. Chem. Chem. Phys.*, 2002, **4**, 2111–2118.

66 C. Hättig, *Adv. Quant. Chem.*, 2005, **50**, 37–60.

67 A. Schäfer, H. Horn and R. Ahlrichs, *J. Chem. Phys.*, 1992, **97**, 2571–2577.

68 A. Schäfer, C. Huber and R. Ahlrichs, *J. Chem. Phys.*, 1994, **100**, 5829–5835.

69 F. Plasser, TheoDORE*: a package for theoretical density, orbital relaxation, and exciton analysis; available from* `http://theodore-qc.sourceforge.net/`.

70 E. Hennebicq, C. Deleener, J.-L. Bredas, G. D. Scholes and D. Beljonne, *J. Chem. Phys.*, 2006, **125**, 054901.

71 A. B. Trofimov, G. Stelter and J. Schirmer, *J. Chem. Phys.*, 1999, **111**, 9982–9999.

72 A. B. Trofimov, G. Stelter and J. Schirmer, *J. Chem. Phys.*, 2002, **117**, 6402–6409.

73 M. Albota, D. Beljonne, J.-L. Brédas, J. E. Ehrlich, J.-Y. Fu, A. A. Heikal, S. E. Hess, T. Kogej, M. D. Levin, S. R. Marder, D. McCord-Maughon, J. W. Perry, H. Röckel, M. Rumi, G. Subramaniam, W. W. Webb, X.-L. Wu and C. Xu, *Science*, 1998, **281**, 1653–1656.

74 D. Yamaki, Y. Kitagawa, H. Nagao, M. Nakano, Y. Yoshioka and K. Yamaguchi, *Int. J. Quant. Chem.*, 1999, **75**, 645–654.

75 J. Coe and M. Paterson, *Mol. Phys.*, 2014, **112**, 733–739.

76 A. V. Luzanov, D. Casanova, X. Feng and A. I. Krylov, *J. Chem. Phys.*, 2015, **142**, 224104.

77 G. Hohlneicher and B. Dick, *J. Photochem.*, 1984, **27**, 215 – 231.

78 H. Woo, O. Lhost, S. Graham, D. Bradley, R. Friend, C. Quattrocchi, J. Brédas, R. Schenk and K. Müllen, *Synth. Met.*, 1993, **59**, 13 – 28.

79 J. Gierschner, H.-G. Mack, L. Lüer and D. Oelkrug, *J. Chem. Phys.*, 2002, **116**, 8596–8609.

80 J. H. Starcke, M. Wormit, J. Schirmer and A. Dreuw, *Chem. Phys.*, 2006, **329**, 39–49.

81 J. H. Starcke, M. Wormit and A. Dreuw, *J. Chem. Phys.*, 2009, **131**, 144311.

82 S. Knippenberg, J. H. Starcke, M. Wormit and A. Dreuw, *Chem. Phys.*, 2010, **108**, 2801–2813.

83 M. Wohlgenannt, W. Graupner, R. Österbacka, G. Leising, D. Comoretto and Z. V. Vardeny, *Synth. Met.*, 1999, **101**, 267–268.

84 M. B. Smith and J. Michl, *Chem. Rev.*, 2010, **110**, 6891–6936.

85 F. Plasser, S. Bäppler, M. Wormit and A. Dreuw, *J. Chem. Phys.*, 2014, **141**, 024107.

86 S. Kraner, R. Scholz, F. Plasser, C. Koerner and K. Leo, *submitted for publication*.

87 S. Martin, D. Bradley, P. Lane, H. Mellor and P. Burn, *Phys. Rev. B*, 1999, **59**, 15133–15142.

88 E. K. Miller, D. Yoshida, C. Y. Yang and A. J. Heeger, *Phys. Rev. B*, 1999, **59**, 4661–4664.

89 S. V. Frolov, Z. Bao, M. Wohlgenannt and Z. V. Vardeny, *Phys. Rev. B*, 2002, **65**, 205209.

90 A. Köhler and B. D., *Adv. Funct. Mater.*, 2004, **14**, 11–18.

91 A. P. Monkman, H. D. Burrows, L. J. Hartwell, L. E. Horsburgh, I. Hamblett and S. Navaratnam, *Phys. Rev. Lett.*, 2001, **86**, 1358–1361.

92 W. Barford, R. J. Bursill and R. W. Smith, *Phys. Rev. B*, 2002, **66**, 115205.

93 D. Halliday, P. Burn, R. Friend, D. Bradley, A. Holmes and A. Kraft, *Synt. Met.*, 1993, **55**, 954 – 959.

94 J. Gierschner, J. Cornil and H.-J. Egelhaaf, *Adv. Mater.*, 2007, **19**, 173–191.

95 J.-M. Mewes, Z.-Q. You, M. Wormit, T. Kriesche, J. M. Herbert and A. Dreuw, *J. Phys. Chem. A*, 2015, **119**, 5446–5464.